PCCP

View Online

Dynamic Article Links

Cite this: DOI: 10.1039/c1cp22250c

www.rsc.org/pccp

PAPER

Enhanced weak localization effect in few-layer graphene†

Yanping Liu, Wen Siang Lew* and Li Sun

Received 11th July 2011, Accepted 9th September 2011
DOI: 10.1039/c1cp22250c

We have investigated the weak localization correction to magnetoresistance in one to six layer graphene structures. The magnetoresistance measurements have revealed that, in addition to the known transition from weak anti-localization in monolayer graphene to weak localization in bilayer graphene, the weak localization effect becomes more pronounced as the number of graphene layers increases. The obtained results substantiate that because few-layer graphene suppresses mesoscopic corrugations and increases intervalley scattering it leads to the observed enhancement of negative resistance, resulting in the restoration of the weak localization in graphene materials. High field magnetoresistance measurements show non-linear behavior, which indicates the breaking of sub-lattice symmetry and the formation of excitonic gap in the Landau level.

1. Introduction

Graphene has shown remarkable quantum interference properties because its low-energy excitation is massless Dirac fermions and this quasi-particle is chiral in nature.[1–3] This property is attributed to the fact that two valleys of Dirac-like chiral quasi-particles with isospin in the hexagonal lattice exhibit Berry phase π with respect to the momentum direction.[4–6] Hence, graphene has unique quantum interference behavior compared to the conventional two-dimensional systems. Owing to the chirality feature of its electrons, it is not only dependent on inelastic and phase-breaking scattering, but also on a number of elastic scattering processes.[7] The accumulation of Berry phase π changes the sign of the amplitude in the time-reversed path, resulting in a suppression of backscattering as the two paths interfere destructively.[8–10] Therefore, one expects a positive magnetoresistance (MR) when the scattering between valleys in monolayer graphene is neglected.[11–13] For bilayer graphene, due to the massive chiral quasi-particles with a parabolic dispersion and a different degree of chirality with respect to Berry phase 2π, the backscattering is not suppressed and that leads to the conventional weak localization.[14,15] Generally, intravalley and intervalley elastic scattering can be represented by two different scattering times τ_{intra} and τ_{inter}. If $\tau_{intra} \leq \tau_{inter}$ one expects weak anti-localization (WAL), whereas for $\tau_{intra} \geq \tau_{inter}$, weak localization (WL)[7,8] is obtained. Recently, three and higher numbered layer graphene structures have attracted significant attention because the layer stacking configurations give rise to novel electronic interactions.[16–18] The unusual electronic transport properties have shown remarkable application potential in nanoelectronic devices.[19–22] However, the understanding of quantum interference correction to the magneto-transport in few-layer graphene (FLG) is not fully established yet. Specifically, the influences of the nature of disorder and the mesoscopic ripple on the quantum interference transport properties are of particular interest. Hence, a better understanding of the general quantum interference transport property of few-layer graphene is necessary.

In this paper, we report on the systematic study of the weak localization effect in few layer graphene; from monolayer to six-layer. Our investigation reveals that the effect changes from weak anti-localization to weak localization for the transition from one to two layers, and the weak localization effect becomes more pronounced as the number of graphene layers is increased beyond two. As the number of graphene layers increases, the weakening ripple effect causes the intervalley scattering to be more dominant in determining the weak localization effect. At high field measurement the measured magnetoresistance (MR) increases non-linearly with the applied field strength. The obtained result implies that the excitonic gap in few layer graphene is thermally activated.

2. Methods

Graphene layers were produced using mechanical exfoliation techniques[5] from the bulk highly oriented pyrolitic graphite (grade ZYA, SPI Supplies) on Si/SiO_2 (300 nm) substrates. Optical microscopy was used to locate the graphene flakes. Four contact electrodes were fabricated using standard optical lithography techniques and deposition of Cr (10 nm)/Au (80 nm) films was carried out *via* thermal evaporation under 10^{-7} mbar conditions. Electronic transport measurements were conducted on multiple samples, using PPMS (Quantum Design) with a fixed

School of Physical and Mathematical Sciences, Nanyang Technological University, 21 Nanyang Link, Singapore 637371. E-mail: wensiang@ntu.edu.sg
† Electronic supplementary information (ESI) available. See DOI: 10.1039/c1cp22250c

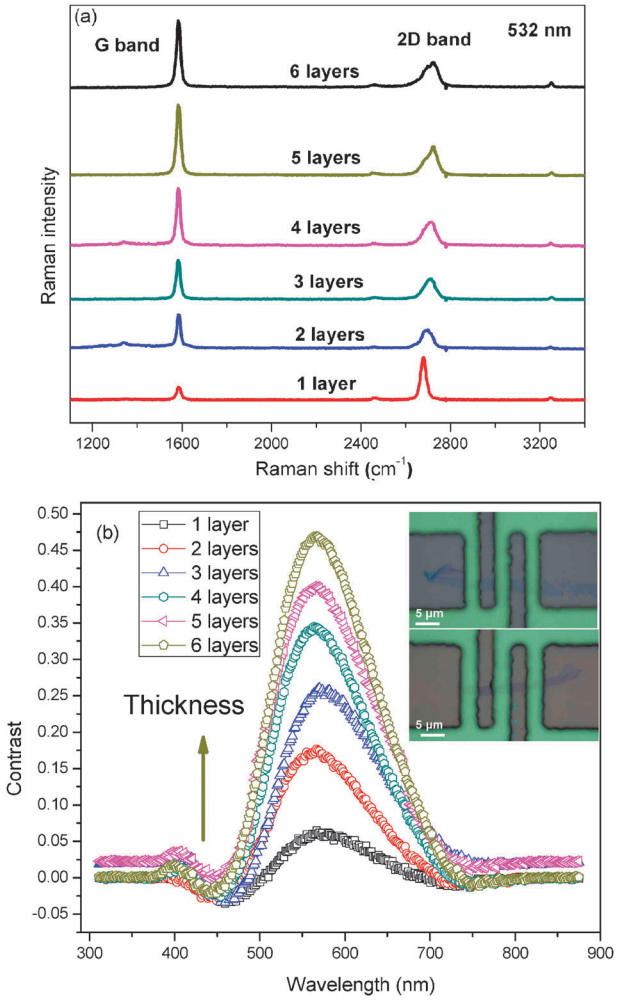

Fig. 1 (a) Comparison of Raman spectra at 532 nm for mono-to six-layer graphene. The position of the G peak and the spectral features of the 2D band indicate the number of graphene layers. (b) Contrast spectrum measurement of mono- and six-layer graphene. Inset in (b) is an optical image of the FLG interconnected with the corresponding metal electrodes.

excitation current of 0.01 mA. For magnetic field measurement, the field was applied perpendicular to the plane of the sample. Thermal annealing was carried out at 300 °C in a vacuum for 3 hours to eliminate contamination and to restore clean surfaces of graphene. *In situ* magnetic and electric fields cycling was carried out to clean the graphene samples. The determination of the number of graphene layers was carried out using the micro-Raman spectroscopy technique *via* the 2D-band deconvolution procedure.[23,24] The Raman spectra were measured at room temperature using a WITEC CRM200 instrument at 532 nm excitation wavelength in a backscattering configuration. Shown in Fig. 1a are the characteristic Raman spectra of the few layer graphene. For all the graphene layers, the Raman spectrum has a distinguishable G peak and a 2D band, which are strongly dependent on the number of graphene layers. By comparing the full-width at half maximum of the 2D band of all the layers, we can confirm the number graphene layers.[25] In addition, we have also carried out contrast spectrum measurement for each graphene sample and the result is shown in Fig. 1b. Comparison among the contrast spectrum could provide a quantitative guide to the visual confirmation of the graphene layers,[26–29] and is consistent with our results from Fig. 1a. An optical image of the FLG interconnected with the corresponding metal electrodes is displayed in the inset of Fig. 1b.

3. Results and discussion

The quantum interference effect present in graphene has a notable difference compared to that in a conventional two-dimensional (2D) system, *i.e.* the chiral nature of the charge carriers and the addition of the Berry phase have led to reduced backscattering.[8–10] Recent theoretical analysis has shown that the quantum interference in graphene is not only dependent on elastic scattering, but also on inelastic scattering, which could affect the phase of the wave function.[7] Scattering between the valleys in graphene and the quasi-exact conservation of the chirality have a profound effect on the low-field magnetoresistance.[8] Fig. 2a illustrates the band structure of graphene. The dotted and solid arrows indicate the intravalley and the intervalley scatterings, respectively. Fig. 2b is an illustration of the trajectory of an electron scattered by impurities that result in quantum correction to the resistance. A pair of time-reserved paths contributes to backscattering: a different direction of electron travel along a closed path induces an accumulation of the geometric phase, which contributes to the interference process. In monolayer graphene, the two paths interfere destructively because Berry phase π leads to the suppression of backscattering.[11–13] Fig. 2c is an illustration of the process responsible for trigonal warping (τ_w^{-1}), intervalley scattering (τ_i^{-1}) and chirality-breaking (τ_z^{-1}). The dashed line is the shape of the hexagonal Brillouin zone of graphene and the solid line of trigonal shape is the Fermi surface at a finite energy in the vicinity of two non-equivalent valleys K_+ and K_-. The trigonal warping effect[15] induces an asymmetry of the electron dispersion at each valley $\varepsilon(K_\pm, \boldsymbol{p}) \neq \varepsilon(K_\pm, -\boldsymbol{p})$, where $\boldsymbol{p}$ is the momentum. The warping effects in the intervalley have opposite signs: $\varepsilon(K_\pm, \boldsymbol{p}) = \varepsilon(K_\mp, -\boldsymbol{p})$. The warping effect of the electron dispersion near the center of each valley breaks the chirality of quasi-particles in the localization properties, which leads to the suppression of WAL and WL effects in the monolayer and bilayer, respectively. However, because of the opposite chirality of the quasi-particles in the two valleys, the chirality-breaking elastic intervalley scattering will restore WL which exhibits negative magnetoresistance behavior in monolayer and bilayer graphene.[11–14]

In Fig. 3 we present low-field magnetoresistance measurement of one to six layer graphene structures at temperatures 2 K, 20 K and 50 K. Our experimental results confirm the known transition of weak anti-localization in monolayer graphene to weak localization effects in bilayer graphene. The origin of the suppression of the weak localization property in monolayer graphene is dependent on the trigonal warping of the graphene band structures, which results in an asymmetry of the carrier dispersion with respect to the center of the corresponding valley. To better analyze our results we choose a model proposed by McCann *et al.*,[8] that the weak localization magnetoresistance is mainly dependent on two types of scattering rates, *i.e.* inelastic (phase-breaking, τ_ϕ) and elastic (chirality-breaking, τ_i, τ_w).

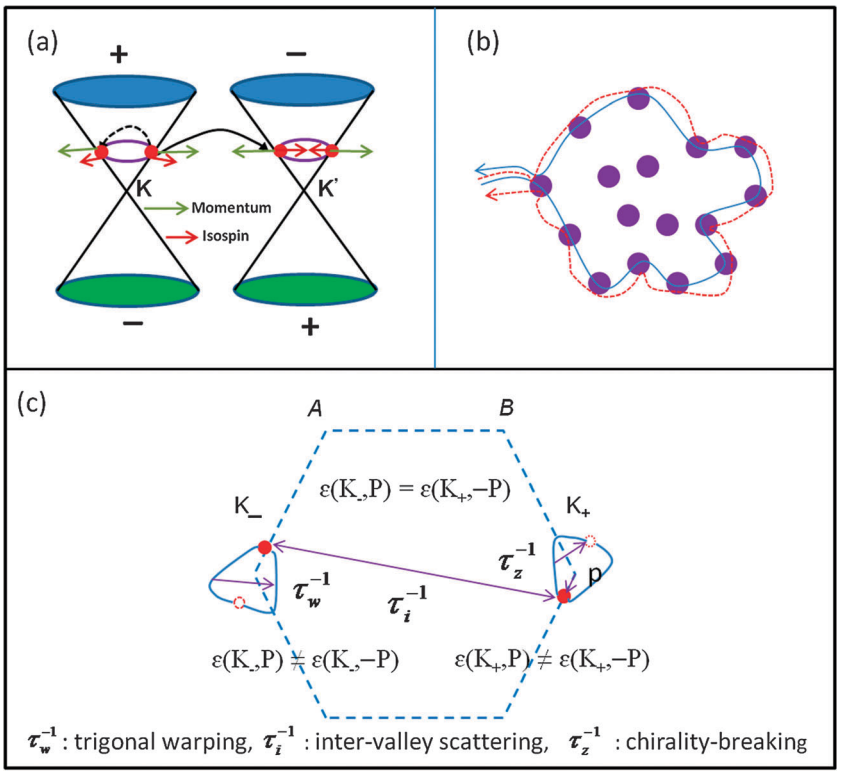

Fig. 2 (a) Schematic of the band structure of graphene, with dotted and solid arrows showing the intravalley and the intervalley scatterings, respectively. (b) Illustration of the trajectories of an electron scattered by impurities that result in a quantum correction to the resistance. (c) Illustration of the process responsible for trigonal warping (τ_w^{-1}), inter-valley scattering (τ_i^{-1}) and chirality-breaking (τ_z^{-1}). The dashed line is the shape of the hexagonal Brillouin zone of graphene and the solid line of trigonal shape is the Fermi surface at a finite energy in the vicinity of two non-equivalent valleys K_+ and K_-. The trigonal warping effect induces an asymmetry of the electron dispersion at each valley $\varepsilon(K_\pm, \boldsymbol{p}) \neq \varepsilon(K_\pm, -\boldsymbol{p})$, where $\boldsymbol{p}$ is the momentum. The effects of the warping in the intervalley have opposite signs: $\varepsilon(K_\pm, \boldsymbol{p}) = \varepsilon(K_\mp, -\boldsymbol{p})$. The trigonal warping time grows as the Fermi energy increases and contributes to the coherent backscattering in the valley.

The magnetoresistance expression of the model is given by:

$$\rho(B)-\rho(0)\equiv\Delta\rho(B)=-\frac{e^2\rho^2}{\pi h}\left[F\left(\frac{2\tau_\phi}{\tau_B}\right)-F\left(\frac{2}{\tau_B(\tau_\phi^{-1}+2\tau_i^{-1})}\right)-2F\left(\frac{2}{\tau_B(\tau_\phi^{-1}+\tau_i^{-1}+\tau_w^{-1})}\right)\right] \quad (1)$$

where $F(z)=\ln(z)+\psi\left(\frac{1}{2}+\frac{1}{z}\right)$. Here, ψ is the digamma function; τ_ϕ is the phase coherence time; τ_i is the intervalley scattering time, where the scattering potential is long-range due to ripples, dislocations and charged scatterers; τ_w is the warping-induced relaxation time that is contributed by the intravalley scattering due to the trigonal warping effect; $\tau_B=\frac{\hbar}{2eDB}$, where D is the diffusion constant. The trigonal warping time grows as the Fermi energy increases and contributes to a certain degree of backscattering in the valley. The first term in eqn (1) is responsible for weak localization, while the second and third terms with negative sign lead to anti-localization. The theory implies that the MR has a sharp peak at $B = 0$ and a positive slope at higher fields. The positive MR shown in Fig. 3a is a clear signature of WAL, as a result of the suppression of the backscattering because of Berry phase π, as well as the suppression of the weak localization due to the trigonal warping effect. Therefore, the results signify the importance of intravalley scattering in monolayer graphene and the long-range scattering that contributes to the preservation of AB sublattice symmetry.

In even numbered layer graphene the total phase around a closed loop is 2π and the backscattering is not suppressed. Therefore, the results show an ordinary weak localization effect. To analyze the even numbered layer graphene results we use the following expression [15] for the magnetoresistance due to WL:

$$\rho(B)-\rho(0)\equiv\Delta\rho(B)=\frac{e^2}{\pi h}\left[F\left(\frac{B}{B_\phi}\right)-F\left(\frac{B}{B_\phi+2B_i}\right)+2F\left(\frac{B}{B_\phi+B_*}\right)\right] \quad (2)$$

where $F(z)=\ln(z)+\psi\left(\frac{1}{2}+\frac{1}{z}\right)$, $B_{\phi,i,*}=\frac{\hbar}{4De}\tau_{\phi,i,*}^{-1}$, and $(\tau_*)^{-1} = (\tau_i)^{-1} + (\tau_w)^{-1}$. The distinctive feature compared to the monolayer graphene is that the third term in eqn (2) has a positive sign. Owing to the presence of an intervalley scattering factor (B_i) in the second term, the first term becomes dominant at small field. This result leads to the observation of a negative magnetoresistance due to the WL effect. The model predicts that such WL correction to magnetoresistance in bilayer graphene is saturated at a magnetic field determined by the intervalley scattering time. This is different from the transport time used in conventional metal structures with respect to the intervalley scattering time τ_i. The negative MR in Fig. 3b is a clear

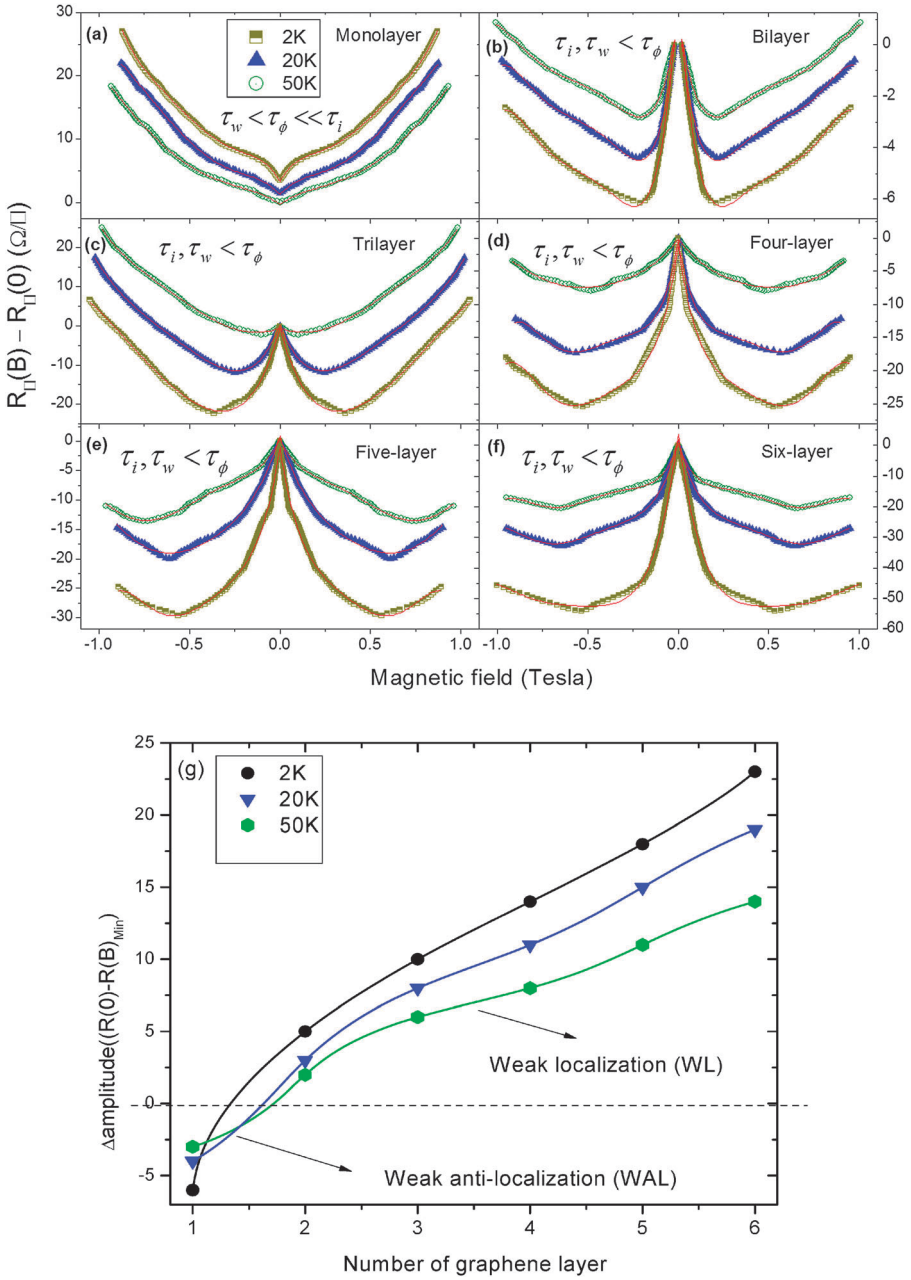

Fig. 3 (a)–(f) Low-field magnetoresistance of mono- to six-layer graphene at temperatures 2–50 K. The measurements reveal a positive magnetoresistance in monolayer graphene and a negative magnetoresistance in few-layer graphene, which correspond to anti-weak localization and weak localization effects, respectively. The weak localization effect becomes more pronounced when the number of graphene layers increases. As the temperature increases the weak localization effect diminishes due to the reduction of the phase coherence time. (g) The relative amplitude of magnetoresistance as a function of the number of graphene layers, the result shows that the weak localization effect has stronger dependence on the graphene layer. The solid line is a guide to the eye.

signature of the WL effect, arising from backscattering as a consequence of the Berry phase 2π. The result signifies the importance of intervalley scattering in bilayer graphene and the short-range scattering that contributes to the breaking of AB sublattice symmetry. For graphene structures with three layers and above, their parabolic band structure is similar to that of bilayer graphene. The few layer graphene is characterized by the chiral quasi-particles property with respect to Berry phase $N\pi$ for N layers. Hence, for odd layer graphene, the backscattering is suppressed due to the odd Berry phase, however, this is not happening in even layer graphene (even Berry phase). Consequently, the low-field magnetoresistance for even layer graphene shows an ordinary weak localization effect. The quantum interference correction to the magnetoresistance in few layer graphene is dependent on the interplay of the intravalley and intervalley scatterings. As the number of graphene layers increases, measurement results shown in Fig. 3c–f indicate that the weak localization effect becomes more pronounced. The enhanced WL effect is ascribed to the suppression of the mesoscopic corrugations and the increase of

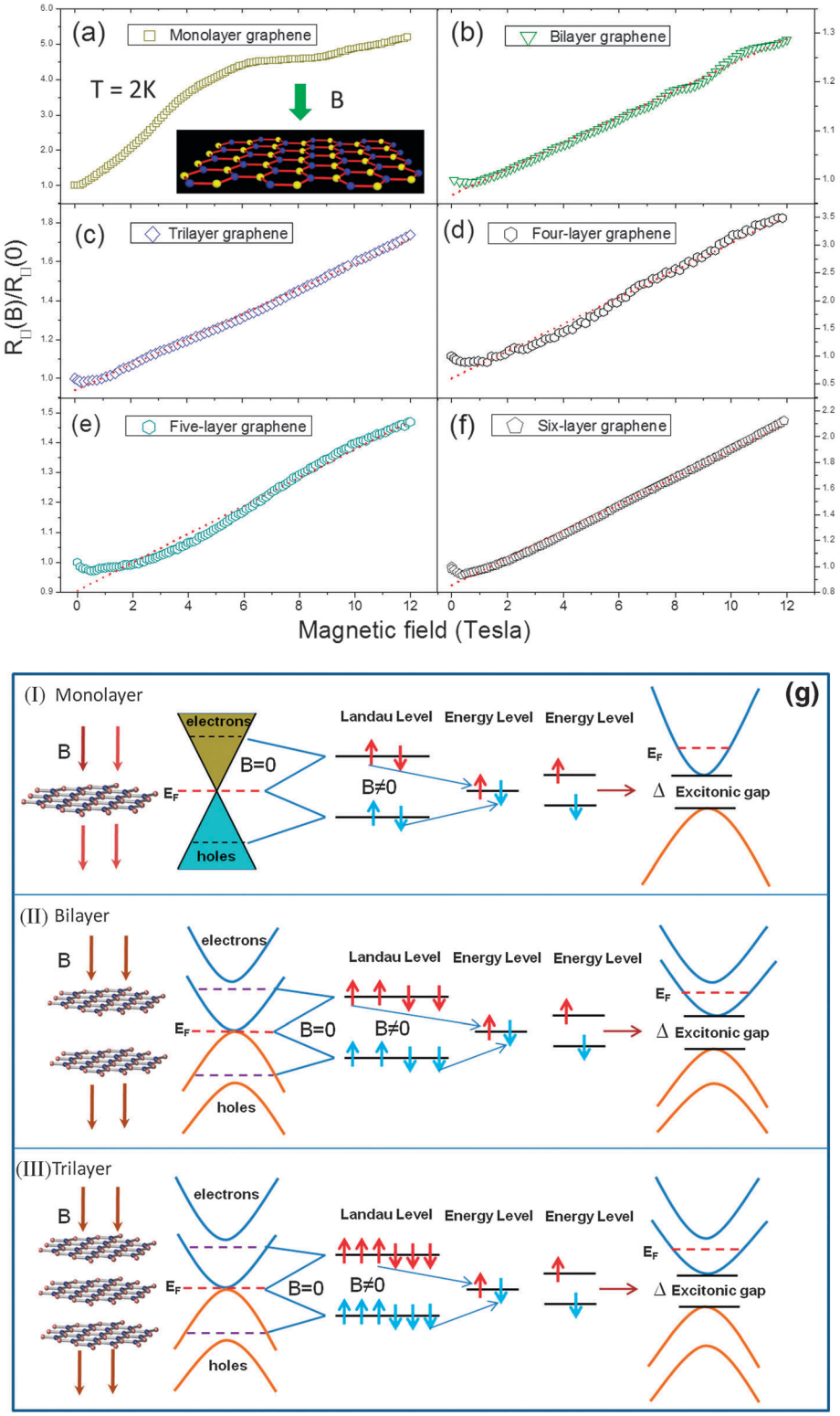

Fig. 4 (a)–(f) Resistance measurements as a function of magnetic field at $T = 2$ K. The measured resistance has a non-linear relationship with the applied magnetic field strength and that can be explained by the concept of Landau level (LL) splitting. The dotted line is the fit following the report that this gap is of excitonic nature and will increase with $\sqrt{B}$. (g) I, II, III are the illustrations of monolayer, bilayer and trilayer graphene bandgaps and the Landau level splitting under the influence of the magnetic field, respectively. The zero-energy state with respect to up-spin electrons and down-spin holes makes an excitation condensation gap because of the attractive Coulomb force between a hole and an electron.

intervalley scattering as more graphene layers are added. More graphene layers directly contribute to the addition of atomically sharp scatters hence increasing the intervalley scattering.[7–10] This leads to a negative magnetoresistance that tries to restore the weak localization in few layer graphene. The quantum interference corrections to the magnetoresistance in graphene diminish as temperature rises. This originates from the reduction of the phase coherence time. At low temperature elastic scattering becomes the dominant mechanism as inelastic scattering is strongly suppressed, which allows electrons to retain their phase coherence over long distances. However, at higher temperature inelastic scattering becomes more dominant than elastic scattering, this results in a phase coherence distance of electron waves smaller than the scattering length. Hence, weak localization is the typical quantum interference effect that arises in graphene at low temperatures.

Fig. 4 shows four-terminal magnetoresistance $R_{\square}(B)/R_{\square}(0)$ measurement of mono-to six-layer graphene as a function of magnetic fields at temperature $T = 2$ K. The measurements show that the magnetoresistance $R_{\square}$ has a non-linear relationship with applied magnetic field strength. The origin of the magnetoresistance increment is that the splitting of the Landau level gives rise to bandgap opening at the zero energy level.[30–32] In monolayer graphene, one of the unique properties of massless Dirac electrons is that it has intrinsic Zeeman energy which is accurately one half of the cyclotron energy in magnetic field. This property leads to the splitting of the Landau-level (LL) energy spectrum and is characterised by four-fold degeneracy at zero and non-zero-energy levels,[33] which leads to the breaking of sub-lattice symmetry and the formation of excitonic gap in the Landau level.[34] In addition, when the Coulomb interaction is accounted, it gives rise to a gap opening at the zero energy level due to the attractive interaction between electron–hole pairs that forms an excitonic condensation gap.[33] Shown in Fig. 4a, b and c are illustrations of monolayer, bilayer and trilayer graphene bandgaps and Landau level splitting under the influence of a magnetic field, respectively. The zero-energy state with respect to up-spin electrons and down-spin holes makes an excitation condensation gap due to the attractive Coulomb force between a hole and an electron. The gap is excitonic in nature and increases with $\sqrt{B}$. In FLGs, each Landau level at energy E_n is assumed to be N fourfold degenerate due to twofold spin degeneracy and twofold sublattice symmetry. As seen from Fig. 4a, there is a strong increase in the resistance in the range of applied field strength 0–6 T. At larger fields (>6 T), $R_{\square}(B)/R_{\square}(0)$ increases in a nonlinear manner, with indication towards saturation. One interesting characteristic in Fig. 4a and b is that the non-linear increments of magnetoresistance $R_{\square}(B)/R_{\square}(0)$ contain a plateau-like phase. One possible explanation for this is the formation of an augmented sublattice spin-splitting due to surface-impurity concentration of the graphene layer.[35] The measured magnetoresistance in three to six-layer graphene differs from that of monolayer and bilayer graphene, *i.e.* non-linear resistance increment without showing plateau-like phases. This is because the surface impurity is significantly screened by an additional graphene layer. In our measurements, we have observed an analytical approximation for the non-linear magnetoresistance $R_{\square} \propto \exp(\sqrt{B}/k_B T)$, where k_B is the Boltzmann constant. Our results reveal that the energy gap in graphene is thermally activated and is proportional to $\sqrt{B}$. These considerations give a qualitative explanation of the non-linear relationship between magnetoresistance $R_{\square}$ and the magnetic field strength.

4. Conclusion

In conclusion, we have investigated the weak localization correction to magnetoresistance in mono-to six-layer graphene. Our measurements confirm that the effect changes from weak anti-localization to weak localization in mono-to bilayer graphene, and reveal a stronger dependence of the WL effect on the number of graphene layers. The WL enhancement in FLGs is ascribed to the suppression of the ripple effect as the graphene layer increases, as well as the increase of the intervalley scattering because of atomically sharp scatters. High field magnetoresistance measurement shows a non-linear behavior, which implies the formation of an excitonic gap in few-layer graphene, and it also shows thermally activated property.

Acknowledgements

This work was supported in part by the NRF-CRP program (Multifunctional Spintronic Materials and Devices) and the Agency for Science, Technology and Research (A*STAR) SERC grant (082 101 0015). The authors thank Dr Cheong (NTU) for useful discussion and Li Yuanqing for their assistance in experimental measurements.

References

1 K. S. Novoselov, A. K. Geim, S. V. Morozov, D. Jiang, M. I. Katsnelson, I. M. Grigorieva, S. V. Dubonos and A. A. Firsov, *Nature*, 2005, **438**, 197.
2 K. S. Novoselov, Z. Jiang, Y. Zhang, S. V. Morozov, H. L. Stormer, U. Zeitler, J. C. Maan, G. S. Boebinger, P. Kim and A. K. Geim, *Science*, 2007, **315**, 1379.
3 P. R. Wallace, *Phys. Rev.*, 1947, **71**, 622.
4 A. K. Geim and K. S. Novoselov, *Nat. Mater.*, 2007, **6**, 183–191.
5 K. S. Novoselov, A. K. Geim, S. V. Morozov, D. Jiang, Y. Zhang, S. V. Dubonos, I. V. Grigorieva and A. A. Firsov, *Science*, 2004, **306**, 666.
6 A. K. Geim, *Science*, 2009, **324**, 1530.
7 F. V. Tikhonenko, D. W. Horsell, R. V. Gorbachev and A. K. Savchenko, *Phys. Rev. Lett.*, 2008, **100**, 056802.
8 E. McCann, K. Kechedzhi, V. I. Fal'ko, H. Suzuura, T. Ando and B. L. Altshuler, *Phys. Rev. Lett.*, 2006, **97**, 146805.
9 K. Ziegler, *Phys. Rev. Lett.*, 2006, **97**, 266802.
10 A. F. Morpurgo and F. Guinea, *Phys. Rev. Lett.*, 2006, **97**, 196804.
11 S. V. Morozov, K. S. Novoselov, M. I. Katsnelson, F. Schedin, L. A. Ponomarenko, D. Jiang and A. K. Geim, *Phys. Rev. Lett.*, 2006, **97**, 016801.
12 F. V. Tikhonenko, A. A. Kozikov, A. K. Savchenko and R. V. Gorbachev, *Phys. Rev. Lett.*, 2009, **103**, 226801.
13 X. S. Wu, X. B. Li, Z. M. Song, C. Berger and W. A. de Heer, *Phys. Rev. Lett.*, 2007, **98**, 136801.
14 R. V. Gorbachev, F. V. Tikhonenko, A. S. Mayorov, D. W. Horsell and A. K. Savchenko, *Phys. Rev. Lett.*, 2007, **98**, 176805.
15 K. Kechedzhi, V. I. Falko, E. McCann and B. L. Altshuler, *Phys. Rev. Lett.*, 2007, **98**, 176806.
16 M. Aoki and H. Amawashi, *Solid State Commun.*, 2007, **142**, 123.
17 C. L. Lu, C. P. Chang, Y. C. Huang, R. B. Chen and M. L. Lin, *Phys. Rev. B: Condens. Matter*, 2006, **73**, 144427.
18 S. Latil and L. Henrard, *Phys. Rev. Lett.*, 2006, **97**, 036803.
19 K. F. Mak, J. Shan and T. F. Heinz, *Phys. Rev. Lett.*, 2010, **104**, 176404.

20 Y. P. Liu, W. S. Lew, S. Goolaup, H. F. Liew, S. K. Wong and T. Zhou, *ACS Nano*, 2011, **5**, 5490.
21 A. A. Avetisyan, B. Partoens and F. M. Peeters, *Phys. Rev. B: Condens. Matter*, 2010, **81**, 115432.
22 Y. P. Liu, S. Goolaup, C. Murapaka, W. S. Lew and S. K. Wong, *ACS Nano*, 2010, **4**, 7087.
23 L. M. Malard, M. A. Pimenta, G. Dresselhaus and M. S. Dresselhaus, *Phys. Rep.*, 2009, **473**, 51.
24 I. Calizo, I. Bejenari, M. Rahman, L. Guanxiong and A. A. Balandin, *J. Appl. Phys.*, 2009, **106**, 043509.
25 Y. F. Hao, Y. Y. Wang, L. Wang, Z. H. Ni, Z. Q. Wang, R. Wang, C. K. Koo, Z. X. Shen and J. T. L. Thong, *Small*, 2010, **6**, 195.
26 Z. H. Ni, Y. Y. Wang, T. Yu and Z. X. Shen, *Nano Res.*, 2008, **4**, 273.
27 A. C. Ferrari, J. C. Meyer, V. Scardaci, C. Casiraghi, M. Lazzeri, F. Mauri, S. Piscanec, D. Jiang, K. S. Novoselov, S. Roth and A. K. Geim, *Phys. Rev. Lett.*, 2006, **97**, 187401.
28 Z. H. Ni, H. M. Wang, J. Kasim, T. Yu, Y. P. Feng and Z. X. Shen, *Nano Lett.*, 2007, **7**, 2758.
29 W. Xuefeng, Z. Ming and D. D. Nolte, *Appl. Phys. Lett.*, 2009, **95**, 081102.
30 N. M. R. Peres, *Rev. Mod. Phys.*, 2010, **82**, 2673.
31 Y. Zhang, Z. Jiang, J. P. Small, M. S. Purewal, Y. W. Tan, M. Fazlollahi, J. D. Chudow, J. A. Jaszczak, H. L. Stormer and P. Kim, *Phys. Rev. Lett.*, 2006, **96**, 136806.
32 D. V. Khveshchenko, *Phys. Rev. Lett.*, 2001, **87**, 206401.
33 M. Ezawa, *J. Phys. Soc. Jpn.*, 2007, **76**, 094701.
34 A. J. M. Giesbers, L. A. Ponomarenko, K. S. Novoselov, A. K. Geim, M. I. Katsnelson, J. C. Maan and U. Zeitler, *Phys. Rev. B: Condens. Matter*, 2009, **80**, 201403.
35 V. Krstić, D. Obergfell, S. Hansel, G. L. J. A. Rikken, J. H. Blokland, M. Ferreira and S. Roth, *Nano Lett.*, 2008, **8**, 1700.